Dynamic Wireless Power Transfer for Cost-Effective Wireless Sensor Networks Using Frequency-Scanned Beaming

MIGUEL POVEDA-GARCÍA[1], **JORGE OLIVA-SÁNCHEZ**[1], **RAMON SANCHEZ-IBORRA**[2], **DAVID CAÑETE-REBENAQUE**[1], **AND JOSÉ LUIS GÓMEZ-TORNERO**[1], (Senior Member, IEEE)

[1]Department of Information and Communication Technologies, Technical University of Cartagena, 30202 Cartagena, Spain
[2]Department of Information and Communication Engineering, University of Murcia, 30100 Murcia, Spain

Corresponding author: Miguel Poveda-García (miguel.poveda@upct.es)

ABSTRACT A simple adaptive 1-D frequency-scanning method is proposed for radiative wireless power transfer (WPT) systems in low-power wireless sensor networks (WSNs). As a proof of concept, a directive leaky-wave antenna that scans 1-W output RF power in the angular range from $\pm10°$ at 2.4 GHz to $\pm37°$ at 2.5 GHz, is used to power a WSN covering an area of 1.2 m × 1.2 m. It is shown that, using a frequency-scanned antenna, a wider area than using a non-scanned directive antenna can be powered without additional expensive equipment. The WPT protocol is described, showing that any sensor in the WSN can select the optimum transmission channel in the 2.4-GHz band, based on the received signal strength indicator measurements, as the coordinator performs a scheduled frequency hopping phase. This maximizes the WPT beaming efficiency and the transferred dc power. The optimum channel selection can be performed periodically, which makes the system robust against channel state changes.

INDEX TERMS Adaptive beaming, frequency-scanned antennas, radiative wireless power transfer, wireless sensor network.

I. INTRODUCTION

Far field (radiative) wireless power transfer (WPT) is a promising general technique to remotely power mobile devices over relatively long distances [1]–[3]. Due to safety power restrictions and low conversion efficiencies, radiative WPT (RWPT) is mainly considered nowadays for low-power devices and wireless sensor networks (WSN) [4]. Although nondirective antennas can be appropriate to energize sensors that transmit data at very low duty cycles [1], high-gain directive transmitting antennas are mandatory for more power-demanding sensors and/or to increase the maximum distances that can be remotely powered [5]. When using directive antennas, and since the exact position of the sensors might not be known or multiple sensors have to be energized, adaptive beam-forming techniques are being used to focus the radiated power at the desired direction [5]–[7]. This is usually done with complicated two-dimensional (2D) tracking mechanisms, based on MISO (Multiple Input Single Output) [8] phased-array antennas [9] or retrodirective arrays [10]. In these cases, the antenna array architecture is

quite complex, since it requests mixed RF/digital reconfiguration circuitry to control the array weight/feeding coefficients [8], [9]. Also, optimum beam-forming is achieved from instantaneous Channel State Information (CSI) [11]–[13], which is not generally available in low-cost WSN architectures without extra costly hardware.

In this paper, we propose a cost-effective RWPT solution to power a WSN using simple one-dimensional (1D) frequency-scanned directive antennas. The adaptive beaming does not need costly phased-arrays and associated complex digital architecture / weighting optimization algorithms. A single antenna element with two feeding ports is able to adaptively optimize the remote transfer of power for each sensor node, by simply frequency hopping the transmitting signal. The concept is demonstrated for a IEEE 802.15.4-based WSN operating in the 2.4 GHz band, which allows for channel hopping through its 16 existing frequency channels. It is shown how a 5 × 5 sensor grid covering an area of 1.2 m × 1.2 m is efficiently powered using a simple channel selection algorithm based on the Received Signal

TABLE 1. Comparison between different solutions.

Ref.	Antenna Tx/Rx	Freq (GHz)	Range or Power Density achieved	beamforming	Complexity Processing/hardware
[1]	Rectenna, Planar (patch or dipole)	1.96/2.4 GHz	20-200 µW/cm2	Nondirective	Low/medium
[18]	Microstrip patch antenna (Rx)	5.5 GHz	2.55 mW/cm2 (maximum)	Nondirective	Medium/Medium
[13], [15]	Multiuser MISO SWIPT	NA	Assume 40 dB signal attenuation, 5 m	ZF	Medium/ high
[9]	Multiuser MISO SWIPT	NA	5 m (simulated)	ZF and SINR-optimal	Medium/high
[10]	Array, 4 microstrip antennas	2,08 GHz	50 cm	Retro-reflective Direction finding	Low/high
[20]	Array (16)	NA	NA	Multiple harmonic beamforming	Medium/high
[21]	Array	2.45 GHz	NA	Linear time-modulated array	Medium/medium
[22]	2D Van Atta Array. Slot array (Rx)	5.8 GHz	NA	Retrodirective antenna	Low/medium
[23]	Retrodirective dipole antenna array (Tx)	Frequency of GHz (0.915-24)	Less than 1 W/cm2	Retrodirective antenna	Medium/high
[24]	Retrodirective rectenna array (Rx)	5.8 GHz	10 mW/cm2	Retrodirective antenna	Medium/medium
[25]	Retrodirective arrray (Tx)	5.2 GHz	1 m	Circularly Polarized Retrodirective Antenna Array with EBG Structures	Medium/medium
[26]	Array (8)	0.920 GHz	1,5 m	Multiple beam splitting	High/high
[27]	Array antenna (Tx)	2.45 GHz	NA	Switched radiation beam	Medium/Medium
[28]	Array antenna(Tx) Array patch antenna (Rx)	2-4 GHz	0.2-1.5 m	NA	Medium/High
This work	Leaky-Wave Antenna (Tx)	2.45 GHz	1.5 m to the furthest coverage point	1D Frequency scanned	Low/Low

Strength Indicator (RSSI), which is directly provided by the WSN architecture without any extra hardware. Theoretical and experimental results illustrate the proposed concept, demonstrating superior overall beaming efficiency and power transfer performance in the WSN area, when compared to the use of a fixed directive panel antenna.

The rest of the paper is organized as follows. Section II reviews the related work regarding beamforming optimization for WPT. In Section III, the frequency-scanned fan beaming concept is presented. The LWA used to achieve the frequency scanning is presented in Section IV. After that, Section V shows how the antenna can be used in a practical WPT system based on IEEE 802.15.14 wireless standard. Measurements are presented in Section VI. The proposed WPT protocol is explained in Section VII and at the end, in Section VIII some conclusions are shown.

II. RELATED WORK
The most recent efforts devoted to enhance beamforming optimization seek to improve energy transmission through

mathematical algorithms and novel hardware configurations [12], as well as the efficient use of the radio channel, which is shared between information and energy transmissions (Simultaneous Wireless Information and Power Transfer, SWIPT) [9]. One of the most employed solutions consists of complex phased-array antennas with the aim of increasing energy transfer [13]–[17], disregarding the highly desirable low-cost factor in low-power WSNs. These and other solutions are described in Table 1, which shows a comparison of recent proposals to increase the beaming efficiency for RWPT. Since the receiving (Rx) antennas are generally omnidirectional to minimize the cost and size of the sensors, it is the transmitter (Tx) antenna the one that can increase the overall RWPT system beaming efficiency. Observe that the first antenna implementations tried to use non-directive antennas in order to cover big areas but getting ultra-low energy values, appropriate for sensors that transmit at low duty cycles [1]. This work discussed the sensor platform, and pointed out the required codesign of the RF powering and the power management circuits for

optimal performance. In turn, [18] proposed a circularly polarized microstrip antenna that operates as a rectenna for wireless battery charging and data telemetry in close frequency bands around 5 GHz.

More recent studies presented algorithms based on multi-antenna base stations to simultaneous optimize wireless information transmission and power transfer [9], [13], [15]. For instance, the proposal in [15] assumed a multiuser MISO downlink system and common zero-forcing (ZF) beamforming scheme, in order to propose a simplified energy efficiency optimization algorithm under two constraints: the signal-to-interference-plus-noise ratio and the energy harvesting. Based on a similar MISO scenario, [13] and [9] aimed to optimize the weighted sum-powered harvested by the receiver. In general, all these MISO techniques involve complex phased-arrays of antennas to optimize the transmitted beam toward the receiving target. However, they might be too expensive in the context of cost-effective WSN solutions. In this sense, the number of elements of the Tx phased-array can be reduced using Bayesian compressive sensing [19], in order to reduce the antenna complexity and to make easier practical implementations. A different strategy to optimize the Tx beaming efficiency is by the use of time-modulated antenna arrays. In this line, [20] took advantage of the pulse splitting technique in order to determine the optimal split pulse sequence aimed at synthesizing multiple patterns at the central frequency and at an arbitrarily selected harmonic frequency. An interesting approach in this framework can be also found in [21], where a two-step real-time beaming implementation of a linear time-modulated array was applied to envisage a smart WPT system. First, the position of the devices to be energized is determined through a monopulse function. Then, these positions are used to set the time control modulating signals of the entire array for real-time beaming to the obtained directions. Note that these solutions result in medium-high complex hardware implementation and processing algorithms for beamforming.

Other interesting contributions that require less signal processing rely on antenna systems capable of automatically tracking the direction of arrival, such as retro-directive antennas [10], [22]–[25]. They typically consist of simple radiating elements in array configuration connected to a circuit network that conjugates the phase of the incident signal in order to transmit in the same direction. The application for wireless power delivery is described in [10], using a mobile device that broadcasts a pilot signal and a four-elements retro-reflective beamforming antenna. Similarly, [22] proposed a 2D Van Atta array to phase-conjugate the impinging wave, reporting wideband operation around a frequency of 5.8 GHz and a wide beamwidth. Additionally, a retrodirective wire-dipole antenna is investigated in [23] for WPT applied to specific environments. Finally, the use of a circularly polarized retrodirective antenna array for RWPT was reported in [25], implementing EBG (Electromagnetic Band Gap) techniques between the antenna elements aiming at

simultaneously improving cost, compactness, and reducing mutual coupling effects.

Recent developments of far-field wireless-powered sensor networks can be found in [26]–[28], composed of multiple sensor nodes. The proposed real-time algorithm in [26] is able to distribute the transmitted power to multiple nodes simultaneously while allowing a control of the consumed power to ensure perpetual operation. Besides, [27] presented a physical realization of a 2.45 GHz WPT system for charging WSN nodes spatially distributed. In this solution, the transmitter is based on a patch array of 4 elements with a switched radiation beam employing a Butler matrix. The receiver uses directional planar Yagi-Uda antenna. Again, the network provides long time operation as each of the WSN node can measure and report its voltage level, so that the more appropriate beam can be switched to cover specific energy demands. Finally, the WPT system proposed in [28] used a 1D parabolic reflector antenna with a linear feeder composed by an array of dipoles as a transmitting section, while the receiving section is composed of a compact rectangular patch 3×4 rectenna array. Table 1 summarizes for each of these RWPT solutions the operation frequency, the average maximum distance in meters that can be remotely powered and/or the RF power density delivered at the sensor nodes, and the type of beamforming technique to maximize the RWPT beaming efficiency, together with the overall system complexity in terms of associated hardware and signal processing requests to provide such beamforming techniques. In contrast with the cited solutions, here we propose a paradigm shift in comparison with the WPT-beaming state of the art. For that, we propose the use of a simple channel-hopping technique for 1D scanning, to dynamically optimize the beaming efficiency in a WSN grid.

To this end, we proposed the use of a Leaky-Wave Antenna (LWA) as the RWPT Tx. LWAs are widely known for its low profile structure, compact size, easy feeding mechanism and high directivity radiation pattern, hence, enabling also the inherent re-direction of the beam direction just by adjusting the signal frequency [29]. As it will be shown in the following sections, the overall coverage range can be extended without complicated signal processing or hardware implementation. Our solution fits a cost-efficient model, high gain power emission, and easy and quick adaptive technique to optimize the RWPT beaming efficiency.

III. FREQUENCY-SCANNED FAN BEAMING FOR WPT

Fig. 1 represents a scenario of a WSN with 25 sensor nodes separated at a distance of 30 cm and spread in a 5×5 grid in the XY plane, thus covering a total area of 1.2 m $\times$ 1.2 m. A directive antenna with gain G^{TX} is located at the center of the WSN grid at a height z $= H = 1$ m. The DC power transferred to any node of the WSN can be estimated with the well-known link-budget equation used in RWPT [4], [5]:

$$P_{DC} = \eta_{RF-DC} \cdot A_{eff}^{RX} \cdot \eta_{RAD}^{RX} \cdot S_{RF}(r, \theta, \varphi) \qquad (1)$$
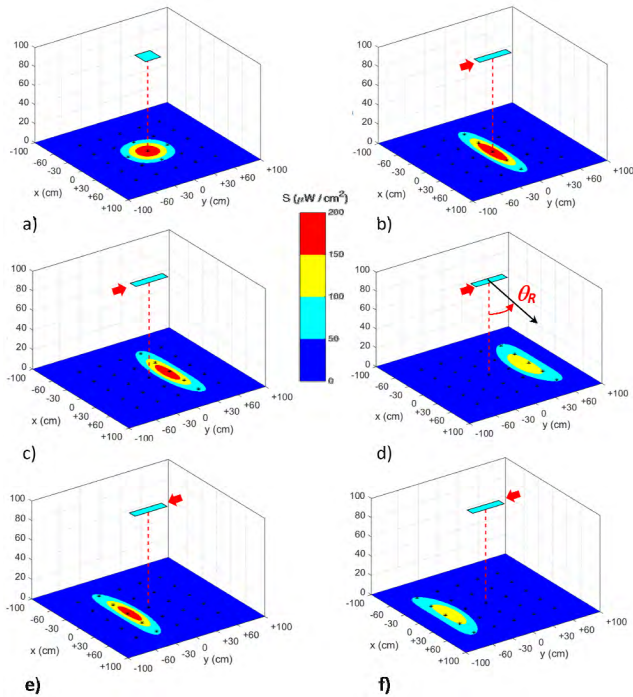
FIGURE 1. Scenario of a 5 × 5 WSN grid powered by a 1 W 14dB gain directive antenna at a height H = 1 m, with different beaming configurations.

and η_{RAD}^{RX} are the effective area and the radiation efficiency of the receiving antenna, and S_{RF} is the microwave power density (W/m^2) at the receiver node, which is given by:

$$S_{RF}(r, \theta, \varphi) = \frac{P_{TX}}{4\pi r^2} \cdot G^{TX}(\theta, \varphi) \qquad (2)$$

where P_{TX} is the transmitted microwave power, and r, θ, φ are the distance and subtending angles between the transmitting antenna and any receiving node position. Unlike long-range point-to-point WPT systems where large collecting antennas are used to maximize the capability to gather the incident power at the receiver [5], $A_{eff}^{RX} \cdot \eta_{RAD}^{RX}$ cannot be maximized in a practical WSN since the nodes must be low-cost and small in size. Similarly, the conversion efficiency η_{RF-DC} is fixed once the harvester circuitry at the sensor node is designed. In WSN RWPT systems, transmitting antenna with high gain G^{TX} are used [1], [4] to intensify the RF power density at the node (2) and therefore enhance the converted DC power (1). The peak gain of this antenna G^{TX} is proportional to its radiation efficiency η_{RAD}^{TX} and its directivity D^{TX}, which is related to the half-power beam width (HPBW) in stereo-radians (the product of the HPBW in each perpendicular plane, $\Delta\theta_X \cdot \Delta\theta_Y$) [30]:

$$G^{TX} = \eta_{RAD}^{TX} \cdot D^{TX} \approx \eta_{RAD}^{TX} \frac{4\pi}{\Delta\theta_X \cdot \Delta\theta_Y} \qquad (3)$$

From (3) it is easy to see that, as we increase the peak gain of the transmitting antenna in a WPT system (keeping the same transmitted power P_{TX}), the antenna becomes more directive as it covers a lower angular region $\Delta\theta_X$, $\Delta\theta_Y$. As a

result, the antenna can power a lower number of nodes. This is illustrated in Fig. 1(a), where a 14 dB gain antenna with HPBW of $\Delta\theta_X = 30°$, $\Delta\theta_Y = 30°$ (16.5 dBi directivity and $\eta_{RAD}^{TX} = 58\%$ radiation efficiency, which is a typical value of commercial panel antennas [31]), transmits RF power of $P_{TX} = 1W$ (+30 dBm) from a height $H = 1m$ above the WSN grid under study. Inserting its angular gain pattern $G^{TX}(\theta, \varphi)$ in (2), the power density distribution along the whole WSN area (XY plane, at a ground level Z = 0) can be numerically computed and plotted. As shown with red color in Fig. 1(a), power densities above 200 μW/cm^2 are obtained just below the transmitting antenna, and this spatial distribution of power radially decays. If we assume a minimum value of 50 μW/cm^2 as the threshold to power our sensor nodes [1], [14], we obtain that only the central 5 nodes within a radius of 30 cm are powered (this limit is shown with cyan contour curve in Fig. 1). In order to power the 20 remaining nodes of the WSN, the directive beam must be focused towards other directions. This can be done with complicated 2D beamforming systems based on costly phased-array antennas [5]–[7] or with a costly mechanical steering system.

Instead of using a directive pencil beam focused in its two planes, we propose for the first time the use of a sectorial-type radiation pattern that is focused in one single plane. In our example, if we use a directive antenna with a HPBW of $\Delta\theta_X = 60°$ and $\Delta\theta_Y = 15°$, the stereo-angle product $\Delta\theta_X \cdot \Delta\theta_Y$ keeps unchanged if compared to the previous example, thus obtaining equal 16.5 dBi directivity and similar 14 dBi gain (and assuming the same radiation efficiency). As a result, similar S > 200 μW/cm^2 peak power density is obtained below the antenna in Fig. 1(b), but now distributed in a narrower region in the y-direction and in a wider area in the x-direction ($\Delta\theta_Y$ has been reduced to half and $\Delta\theta_X$ doubled). Basically, Fig. 1(b) shows a similar amount of 5 sensors with S > 50 μW/cm^2, but now distributed in a single row along the x-direction instead that on the central circle. This fan-beaming configuration has the advantage that simple 1D scanning along the y-direction can be used to illuminate all the 25 nodes of the WSN. This is illustrated in Fig. 1(c) where the antenna scans to an angle of $\theta_R = 10°$ and powers the second row of nodes located at y = +30 cm, while Fig. 1(d) shows the beaming of the third row of nodes at y = +60 cm for a scanning angle $\theta_R = 30°$. The scanning angle θ_R is measured in the ZY-plane as represented in Fig. 1(d). Symmetrically, the row of nodes at y = −30 cm and at y = −60 cm can be illuminated if the transmitting antenna scans to negative angles, $\theta_R = −10°$ and $\theta_R = −30°$, respectively. As a result, the five rows with the total 25 nodes of the WSN can be theoretically powered using simple 1D beam-scanning, thus reducing the complexity if compared to more conventional 2D beam-scanning solutions.

Moreover, 1D scanning can be performed without phased-array antennas and associated electronically reconfigurable feeding hardware (as commonly done with uniform

longitudinal arrays, ULAs [32]–[34]). Effectively, LWAs are known to provide 1D continuous scanning of a directive fan beam by just sweeping frequency and with a simple feeding circuit [29].

IV. 1D SCANNING PLANAR LEAKY-WAVE ANTENNA

As previously commented, one of the main characteristics in the performance of LWAs is their inherent frequency scanning behaviour, known as the antenna dispersion, which consist on the change in the antenna radiation angle θ_R when the frequency of the feeding input signal varies. First examples of LWAs were based on bulky waveguides [29], but this technology lacks the compactness and integrability. Another option is to use planar technology as microstrip LWAs (MLWA), which are especially low-cost since they can be manufactured using standard printed circuit-board (PCB) techniques and, besides, they are very easy to integrate with other planar technologies. One of the keys in the design of such antennas is to be able to control the frequency scanning, so in the operating band of frequencies, the radiation angle is scanned as desired, although there are some restrictions depending on the technology. LWAs are included in the group of travelling wave antennas, which means that only one port is needed to illuminate a long aperture, taking advantage of a travelling guided wave. This eliminates the need of using complex beam forming networks (BFN) to synthesize a directive beam.

In this case, the half-width MLWA (HMLWA) technology, as in [35], has been chosen for our purpose, due to its simplicity, ease of fabrication and integrability. It consists of a microstrip line working with the first higher mode to achieve radiation. For that, in one side of the line there is a row of vias acting as a perfect electric wall and in the other side there is a radiating edge, as seen in Fig. 2(a), which shows a picture of an array of two HMLWAs fabricated in FR4 substrate ($\varepsilon_r = 4.48$ and $\tan \delta = 0.01$).

The frequency scanning of this antenna is controlled with the substrate characteristics and the antenna width. Since the chosen substrate is FR4 with 1mm thickness, as it is cheap, the only parameter to control the dispersion of the antenna is its width. The width will basically control the frequency band: the lower the width, the higher the operating frequency, so it has to be optimized to work in the 2.4 GHz band. Also, the beamwidth of the radiation pattern in the H-plane (YZ-plane according to Fig. 2(a)) of the antenna is controlled with the antenna length as follows [29]:

$$\Delta\theta(f) \approx \frac{1}{\frac{L}{\lambda_0}\cos\theta_R(f)} \tag{4}$$

where L is the antenna length, λ_0 is the wavelength in vacuum and θ_R the radiation angle which depends on the frequency. In this H-plane, the beam can be very narrow as the antenna is long in the y-direction. In the E-plane (XZ-plane), the beam is very wide, since the aperture in the x-direction is just a radiating edge with a ground plane (the metal sheet in Fig. 2(a)). The H-plane and E-plane definition comes from the fact that the polarization of the antenna is linear and contained in the
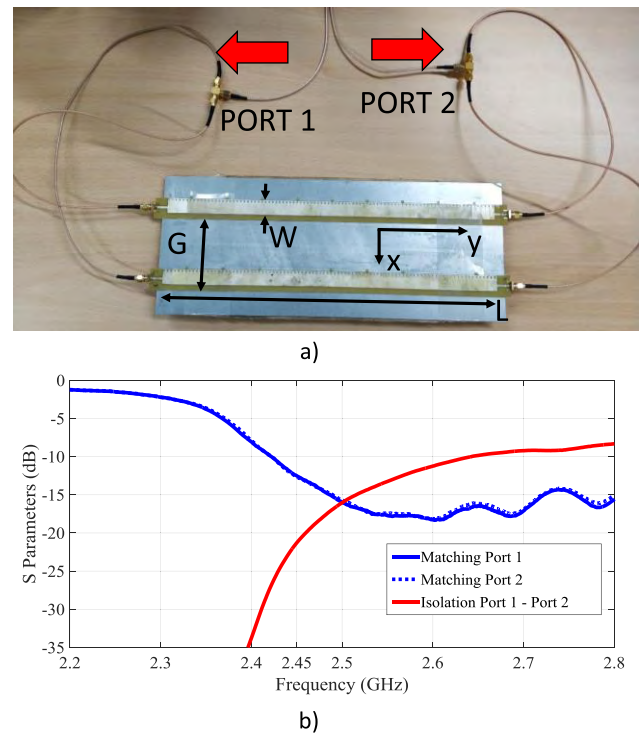

a)

b)

FIGURE 2. Microstrip Leaky-wave Antenna. a) Array of two MLWAs b) S parameters of the array.

TABLE 2. MLWA dimensions.

W (mm)	L (mm)	G (mm)
14.75	520	70

XZ-plane, so the y component of the electric field is negligible compared to the z or x components. In order to reduce the beamwidth in the E-plane, two antennas are arranged in parallel at a distance G in an array configuration in the x-direction, this way, the antenna has a narrower beam [30] in this plane, but wide enough to illuminate all the sensors in a row of the WSN. The reduction in the E-plane beamwidth makes the directivity to increase.

As it can be seen in Fig. 2(a), the feeding network of this antenna is very simple and it just consists of a microstrip line welded to a SMA connector. Also shown in Fig. 2(a), a simple 1:2 power splitter is used to feed the two-MLWA array

To optimize the dispersion and beamwidth of the antenna, the final dimensions, according to the ones in Fig.2 (a), are listed in Table 2.

The reflection coefficient of this antenna (S_{11}) is plotted in Fig. 2(b), showing good input matching $S_{11} < -10$ dB in the whole 2.4-2.5 GHz band, meaning than less than 10% of the power is reflected back to the port. Also, the isolation between the two available ports of the LWA is bellow $S_{21} < -15$ dB, thus assuring that less than 3% of power couples between these two opposed ports.

As depicted in Fig. 3(a), θ_R can be scanned by varying frequency in the ISM band from $\theta_R = \pm 10°$ at 2.4GHz to
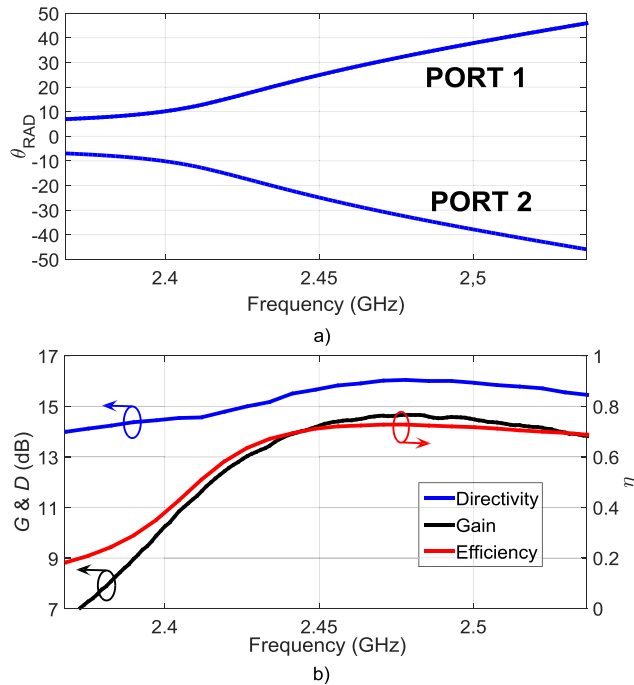
FIGURE 3. Radiation characteristics of the proposed MLWA. a) Radiation angle of the MLWA in the YZ plane as a function of the frequency b) Directivity, gain and efficiency of the MLWA.

FIGURE 4. Radiation patterns of the MLWA. a) H plane for different frequencies b) E plane for different frequencies.

TABLE 3. Radiation pattern characteristics.

Antenna Type	Panel	LWA
Beamwidth	$\Delta\theta_X = 30°$	$\Delta\theta_X = [60° - 90°]$
	$\Delta\theta_Y = 30°$	$\Delta\theta_Y = [16° - 25°]$
Directivity	16.5 dBi	16 dBi
Efficiency	58%	40%-75%
Gain	14 dB	10 dB – 14.7 dB

$\theta_R = \pm37°$ at 2.5 GHz. As previously explained in Fig. 1, positive θ_R values are obtained when the antenna is fed from port 1 in Fig. 2(a) (+y direction), while port 2 provides negative scanning directions (-y direction). The directivity and gain of the antenna can be seen in Fig 3(b) along with the antenna radiation efficiency (η_{RAD}^{RX} in (1)), evidencing they are not constant along the scanning band. This change of the efficiency will make the gain (3) to vary as the beam is scanned, and this will affect the resulting power coverage (2) when using a LWA, as will be explained in Section V.

This frequency-scanning behaviour in the elevation YZ-plane is shown in Fig. 4(a), which shows the normalized radiation patterns for different configurations of the transmitting frequency and feeding port. As shown, the LWA creates a narrow beam in the YZ-plane with a changing beamwidth, that goes from $\Delta\theta_Y = 25°$ to $\Delta\theta_Y = 16°$ as the scanning angle is augmented by increasing transmitting frequency. This narrow beamwidth is achieved thanks to the antenna long size in the y-direction $L = 52$ cm (approximately 4.3 wavelengths at 2.5 GHz). Using two antennas in array configuration, with a 1:2 power splitter (see picture in Fig. 2(a)), a beam in the XZ-plane with an approximate beamwidth of $\Delta\theta_X = 60°$ can be synthesized, as shown in Fig. 4(b). It must be noticed that, conversely to the behaviour in the YZ-plane, the beam is not scanned with frequency in the transverse XZ-plane. Nevertheless, a slight variation of the XZ-plane beamwidth from $\Delta\theta_X = 90°$ to $\Delta\theta_X = 60°$ as frequency is swept from 2.4 to 2.5 GHz, can be observed in Fig. 4(b). As commented in Fig. 3(b), the variation of the beamwidth in the two planes impact the resulting directivity from D =
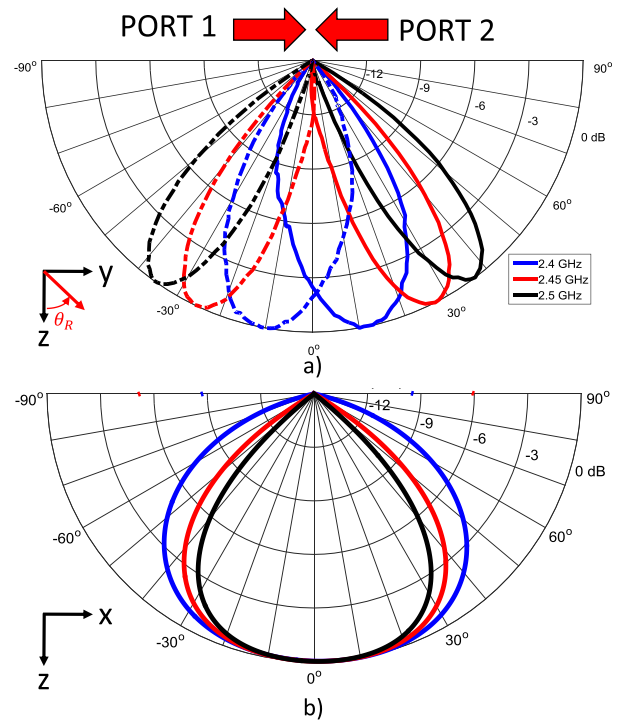
14.5 dBi to D = 16 dBi as the pointing angle is frequency-scanned. Also, the LWA radiation efficiency varies as the beam is scanned with frequency. All these facts result in the peak gain variation shown in Fig. 3(b). The highest peak gain of G = 14.8 dBi is obtained for higher frequencies, where the beam is narrower and thus the radiation more directive, and also the radiation efficiency is higher. All these aspects will affect the final WPT coverage. A summary of these results is presented in Table 3, where the main characteristics of both the panel and the LWA antennas are summarized.

As demonstrated with all these results, this HMLWA creates a 1D frequency-scanned sectorial beam whose scanning angular range, operating bandwidth and resulting beam peak gains, are suitable to demonstrate in the next section the proposed concept of dynamic WPT beaming in a typical WSN operating in the 2.45 GHz ISM band.

V. ADAPTIVE WPT SYSTEM BY FREQUENCY SELECTION
A top view of the WSN scenario under study, with the locations of the 25 nodes and the LWA, is represented in Fig. 5(a).
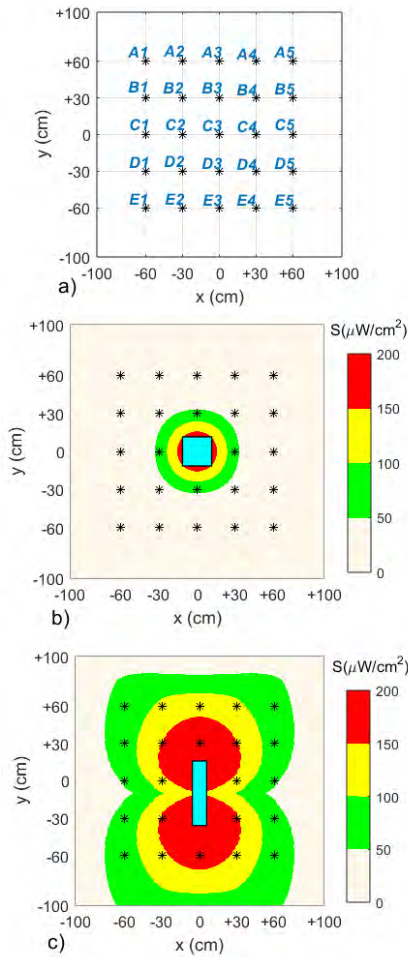
FIGURE 5. WSN scenario under study, top view. a) Nodes location and naming, b) Coverage given by a panel antenna (in blue) with 14 dB gain c) Coverage given by a MLWA (in blue) with gain in Fig. 3b and radiation patterns in Fig. 4.

FIGURE 6. Coverage cut comparison between panel antenna and LWA a) x = 0, b) y = 0.

Each node is codified with a letter to define the rows (from A to E) and a number for the columns (from 1 to 5). In order to demonstrate the usefulness of the proposed scanning LWA, Fig. 5 compares the simulated overall power density coverage when using the fixed-beam directive panel antenna and using the LWA of Table 2 (height $H = 1$ m, transmited power $P_{TX} = 1$ W.

It can be seen in Fig. 5(b) that the coverage provided by the panel antenna (with a directivity of 16.5 dBi, efficiency of $\eta_{RAD}^{TX} = 58\%$ and 14 dBi of gain) will feed just 5 of the 25 nodes (those located at a central circle below the antenna). On the other hand, Fig. 5(c) represents the simulated overall coverage of the MLWA, with the same directivity than the panel antenna (same steradians, as explained in Section III), and with the frequency-beam-scanning described in the previous Section IV. It must be noticed that the coverage of the MLWA plotted in Fig. 5(c), represents the overall power density obtained after the continuous frequency sweep in the 2.45 GHz ISM band, from 2.4 GHz to 2.5 GHz. Besides, it must be noticed that
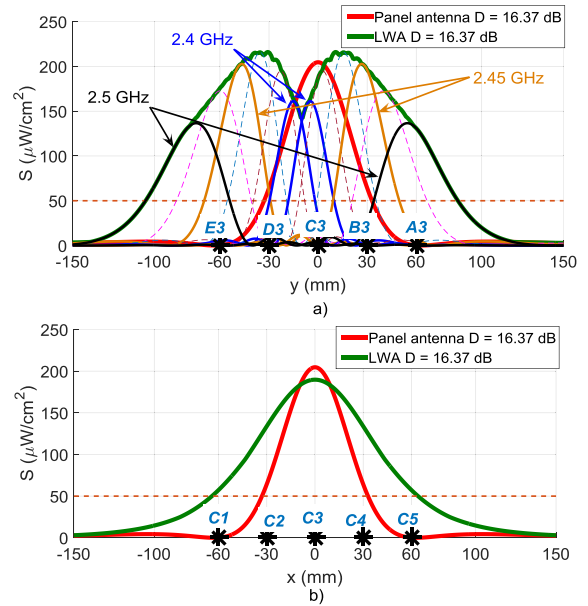
the LWA is not centered with respect to the WSN center (x = 0 cm, y = 0 cm). The MLWA is slightly shifted in the y-axis at x = 0 cm, y = −10 cm, in order to avoid the gain drop associated to perpendicular direction of the antenna (also known as broadside stopband [35]). As it was shown in Fig. 3, broadside direction $\theta_R = 0°$ is associated to the lowest realized peak gain. If the LWA is centered, this perpendicular gain drop would make the center row of sensors to be poorly beamed.

Fig. 6(a) shows the power density cut along the line in the y-direction at x = 0, while Fig. 6(b) represents a cut for the x-direction at y = 0. As illustrated in Fig. 6(a), the overlapping of the different beams that are scanned along y while frequency is varied from 2.4 GHz to 2.5 GHz (represented in dash line with different color for each frequency), is what creates the overall envelope power density coverage along the y-direction. In the case of the x-direction at y = 0, only the first frequency radiates at that line (see Fig.1(b)), hence, only the cut at that frequency is shown.

Clearly, the theoretical results in Fig. 6 demonstrate the superior RF power total coverage produced by the MLWA when sweeping in frequency, if compared to a fixed panel antenna of similar directivity.

VI. MEASUREMENTS
To validate the proposed system, an experimental campaign has been carried out. A 1 W output power amplifier is connected to a microwave signal generator, which can sweep frequency in the 2.45 GHz band. The amplifier output is connected to port 1 or port 2 of the MLWA, as sketched in the scheme of Fig. 7(b). A WPT harvester from Powercast [36] is used to convert incoming RF power to DC at the different locations inside an anechoic chamber as shown in Fig. 7(c).
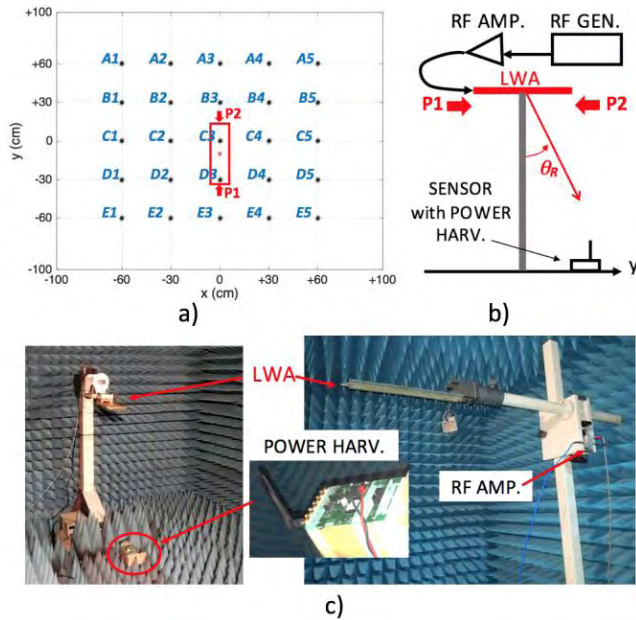
FIGURE 7. Experimental set-up. a) Top view of scenario b) Lateral scheme c) Picture of deployment in an anechoic chamber with detail of harvester and LWA with RF amplifier.

FIGURE 8. Measured results. a) DC duty cycle at the central column as a function of frequency b) Pulsed waveform at the RF-DC converter at D3.

This harvester device transforms received RF power to a pulsed signal whose duty cycle is proportional to the converted DC power which charges the sensor batteries. This pulsed waveform has been captured with a digital oscilloscope as shown in Fig. 8(b). To demonstrate the concept of optimum WPT by frequency sweeping, Fig. 8(a) shows the measured DC duty cycle for the five positions in the central column ($A3 \ldots E3$), as a function of the transmitting RF frequency and by switching the feeding port of the LWA.

As shown in Fig. 8(a), the feeding port of the LWA must be properly chosen, so that nodes at positive y-positions (A3- C3) are powered when port 1 is used, and conversely negative y-positions (D3, E3) must be charged using port 2. Also Fig. 8(a) demonstrates the existence of an optimum frequency for each node location, which maximizes the collected DC power. The selection algorithm employed for choosing the optimum channel for each end-device will be described in the next Section. For instance, the node located at D3 shows maximum duty cycle of 1% when LWA is fed from port 2 and radiates power at 2.42 GHz (this corresponds to the LWA scanning at an angle $\theta_R = -15°$ as shown in Fig. 3(a)). At lower/higher frequencies, the LWA scans at lower/higher angles and thus the radiated beam is not optimally shaped towards the exact spot of the sensor, thus reducing the collected DC power. For this fixed spot D3, Fig. 8(b) depicts the waveforms measured at the RF-DC converter, in a time lapse of 4 s for different transmitting frequencies. As commented, the pulsed waveform shows a higher number of pulses (a lower period between pulses and thus a higher duty cycle), as the collected RF-to-DC power increases. As shown in Fig. 8(b), the signal presents the highest duty cycle at 2.42 GHz (24 pulses in 4 secs), at which
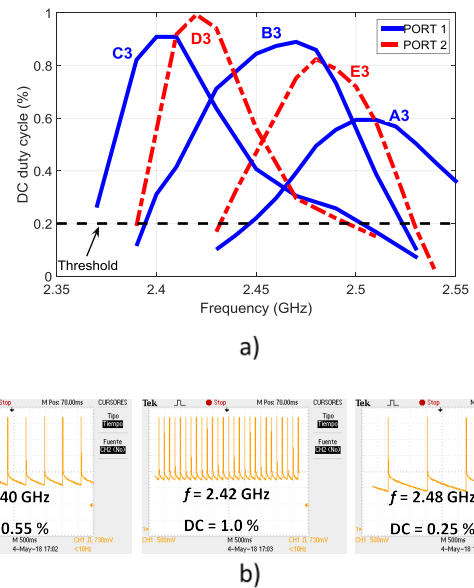
the beaming efficiency between the LWA and the node at D3 is maximized. For other frequencies, the rectified signal shows lower duty cycles since the beam is not optimally focused.

For other locations of the sensor nodes along the y-direction, the optimum RF frequencies shown in Fig. 8(a) shift as expected: higher distances require a higher scanning angle θ_R and hence a higher transmitting RF frequency. The minimum threshold to power the sensors is also marked in Fig. 8(a), indicating that all the five nodes in the central column (in a distance from y $= -60$ cm to y $= +60$ cm) are optimally powered by proper selection of the antenna port and the transmitting frequency from 2.4 to 2.5 GHz. Similar results are obtained for other columns, as shown in Fig. 9(a) for the nodes located at the right-side column ($A5 \ldots E5$). Lower power is transferred in this case since this column is more distant to the transmitting antenna than the central column. Also, the behavior as we move along a row is illustrated in Fig. 9(b), showing the performance of the WPT for the further row ($A1 \ldots A5$). Now only port 1 is used and the optimum frequency is essentially the same for all nodes (around 2.49 GHz), since the beam must be focused to an almost similar scanning angle $\theta_R \approx 35°$ for any position in the same row.

According to these values, a theoretical 2D map of the duty cycle can be represented. For that, the theoretical values of the power density (Fig. 5) are transformed to duty cycle values by a normalizing rectification factor K obtained from the experimental results obtained at node D3. As its duty cycle is 1% (see Fig. 8(a)) for a theoretical power density value $S = 216.12 \mu W/cm^2$, the transformation factor is:

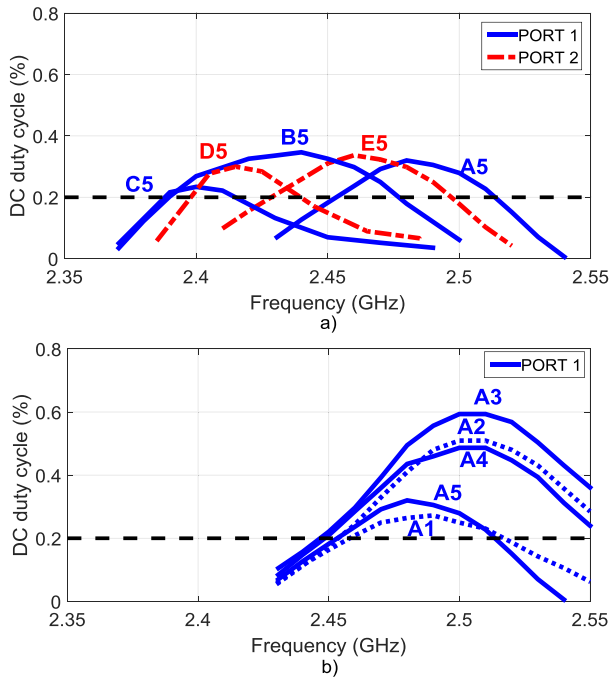$$K = \frac{DC}{S} = 4.63 \cdot 10^{-3} \quad cm^2/\mu W \tag{5}$$

FIGURE 9. Measured DC duty cycle as a function of frequency a) at the right-side column b) at the first row of nodes (further row).

FIGURE 10. Theoretical DC duty cycle on the plane containing the WSN for a) panel antenna b) LWA.
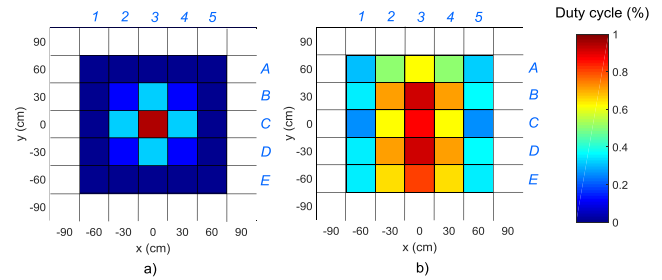

FIGURE 11. Measured DC duty cycle for each node of the WSN a) panel antenna b) LWA.

TABLE 4. Optimal port and frequency (GHz) for each node.

A1	A2	A3	A4	A5
P1 | 2.49	P1 | 2.5	P1 | 2.5	P1 | 2.5	P1 | 2.48
B1	**B2**	**B3**	**B4**	**B5**
P1 | 2.44	P1 | 2.45	P1 | 2.47	P1 | 2.45	P1 | 2.44
C1	**C2**	**C3**	**C4**	**C5**
P1 | 2.4	P1 | 2.4	P1 | 2.4	P1 | 2.4	P1 | 2.4
D1	**D2**	**D3**	**D4**	**D5**
P2 | 2.42	P2 | 2.42	P2 | 2.42	P2 | 2.42	P2 | 2.42
E1	**E2**	**E3**	**E4**	**E5**
P2 | 2.45	P2 | 2.47	P2 | 2.48	P2 | 2.47	P2 | 2.46

Using this approximate linear transformation, Fig. 10(a) shows the theoretical 2D map that predicts the maximum duty cycle expected at each node of the WSN, when the 14 dBi gain panel antenna radiates 1 W. The same is shown in Fig. 10(b) for the designed MLWA, when the proper optimum frequency is selected for each node position. These theoretical results are just a unit conversion (from RF power density to harvested DC), of the simulated power density fingerprints shown in Fig. 5. To check the validity of these simulated results, Fig. 11 shows the measured DC for these two scenarios. Fig. 11(a) represents the DC measured at the 25 nodes when using the 14 dBi gain panel antenna a 1 W RF power, showing that only the central nodes produced a DC above the threshold of 0.2%. On the contrary, the DC measured when using the MLWA in Fig. 11(b), reports that all the 25 nodes harvest RF power with DC well over the threshold. In both cases, good agreement is observed between experiments in Fig. 11 and theoretical results in Fig. 10, demonstrating the superior power coverage provided by the

proposed LWA frequency-beaming WPT scheme when compared to a more conventional directive fixed panel antenna of similar gain. Clearly the LWA allows to power all the 25 nodes in the WSN area of 1.2 m × 1.2 m, while the fixed panel antenna powers only the central nodes.

As commented, to obtain these results we have assumed that each node is remotely powered from the Tx LWA by proper selection of its optimum frequency. Table 4 represents this correspondence between each one of the 25 node positions in Fig. 5(a), and the optimum transmitting frequencies provided by the studied frequency-scanning MLWA. Also, the adequate transmitting port (1 or 2) for each node is summarized in Table 4.

As expected, the optimum frequency increases as the nodes are further located from the WSN center (C3), with respect to the longitudinal y-direction (as we move from one row to another row of nodes). Also it can be seen how, as we get further from the antenna, the difference for the optimal frequency between nodes in the same row increases, so that nodes at central positions (for instance A3) report a higher frequency than those nodes at the edges (A1 and A5, when compared to A3). This is due to the boomerang-shape projected radiation pattern fingerprint, as illustrated in Fig. 1(d).

Finally, in order to show the overall cost of this system, the estimated price of all components is summarized in Table 5. It can be seen that the estimated total cost of the system is around 1311.15 €, shown just as a reference. The cost-effective characteristic of our proposed system comes from the fact that we are using a passive antenna that electronically scans the main beam by just using frequency hopping. Other alternatives, such as the more conventional ULAs would require, for the same antenna length of around $4\lambda_0$

TABLE 5. Cost of the components involved in the WPT system.

Component	Price
Antenna manufacturing	500 €
Zigbee MiMo coordinator [37]	400 €
DC source [38]	400 €
RF power amplifier [39]	10 €
Switch RF [40]	1.15 €

(to achieve the same beamwidth of 15°), a minimum total amount of 9 radiating elements separated a distance λ/2 from each other (to avoid unwanted grating lobes [30]). Thus, a fixed-frequency electronically beam-scanned ULA would require a complex beamforming network (BFN [41]) with 9 pairs of associated electronically tunable phase shifters and attenuators (one per each radiating element), in order to provide similar electronic fan-beam scanning. This makes these systems more expensive because of the need of complex circuitry control for the active antenna to achieve the same scanning capability. Possibilities based on mechanical positioners would need complex and bulky hardware; besides there is a delay associated to the time the positioner takes to mechanically change the pointing direction of the antenna, and also the cost due to mechanical system maintenance. Moreover, it is not possible with a mechanically-steerable directive antenna, to synthesize several simultaneous directive beams. On the contrary, the proposed channel-hopping architecture, can also be used in a multiple beaming mode, so that a multi-tone power RF signal [42]–[44] can be used to simultaneously illuminate several spots. All these aspects will be treated in future works, and they are out of the scope of this first demonstration of the proof-of-concept of our innovative RWPT system.

VII. WPT PROTOCOL

As described above, the proposed WSN WPT system enables the use of optimum beaming if the transmitter is capable of choosing the appropriate frequency channel that maximizes the power transfer for any node in the network. Therefore, this required correspondence (node position – frequency channel) should be dynamically managed by the end-nodes and the energy transmitter by using a simple frequency-selection scheme. To this end, two well-differentiated phases have been defined and integrated within the regular functioning of the WSN, as sketched in Fig. 12. Firstly, at a primary stage called synchronization, each node sniffs the radio channel and measures the received RSSI while the WSN coordinator, i.e., the energy transmitter, executes frequency sweeping and switches between port 1 and 2 of the LWA. The WSN coordinator must introduce a data header to identify the port and frequency channel which are being used (in most wireless protocols the channel ID is provided by default). This process permits end-devices to select the most proper channel regarding received power (RSSI), which depends on their individual positions with respect to the coordinator. Thus, each new node joining the WSN sends a request message to
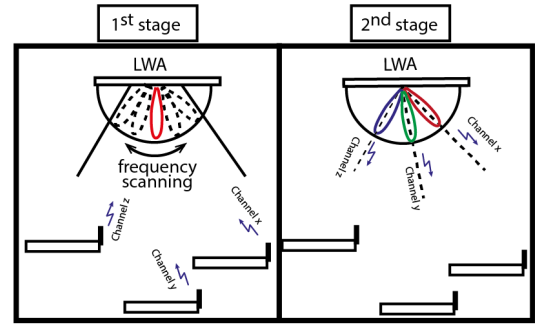

FIGURE 12. WSN synchronization process. a) First stage, coordinator transmits with channel sweeping and end-nodes sniff and select channel for maximizing RSSI. The selected channel is retransmitted by each node to the coordinator. b) Second stage, coordinator performs energy transmission to end-nodes using pre-selected channels.
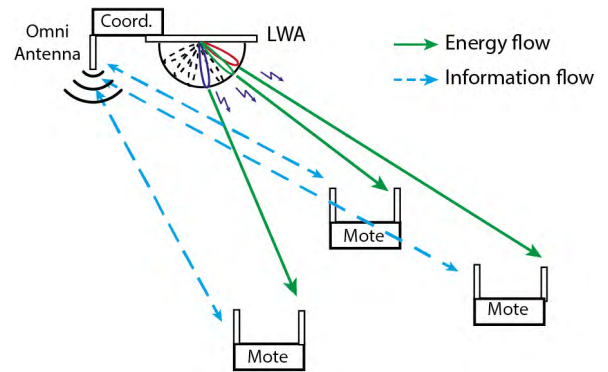

FIGURE 13. WSN scenario: IEEE 802.15.4 MiMo coordinator powering end-nodes through a LWA using pre-selected channels; data links established using omnidirectional antennas.

begin this process and waits till the WSN coordinator starts the synchronization process.

After this first synchronization stage, the second phase corresponds to the powering process of the WSN motes, balancing data and power frames in order to reach acceptable energy-harvesting levels but without severely harming the performance of the data network [9]. As discussed previously, many approaches may be selected with the aim of balancing the transmission of data or energy through the wireless links, which is not the focus of this work [45]. In the following, we illustrate the functionality of the proposed synchronization and powering scheme in a real scenario.

As sketched in Fig. 13, the WSN coordinator as well as the end-devices present two different antennas. Regarding the former, for instance an IEEE 802.15.4-based MiMo 3 × 3 coordinator [37] may be connected to the two ports of the proposed LWA for transmitting energy and to an omnidirectional antenna for sending data traffic. Note that both antennas are connected to the data transmission circuit of the coordinator's hardware. Particularly, the RF power amplifier is connected only to the LWA. On the other hand, two omnidirectional antennas may be attached to the motes, each of them devoted to receive energy or data, separately. Therefore, one antenna is connected to the data transmission circuit of the mote, while
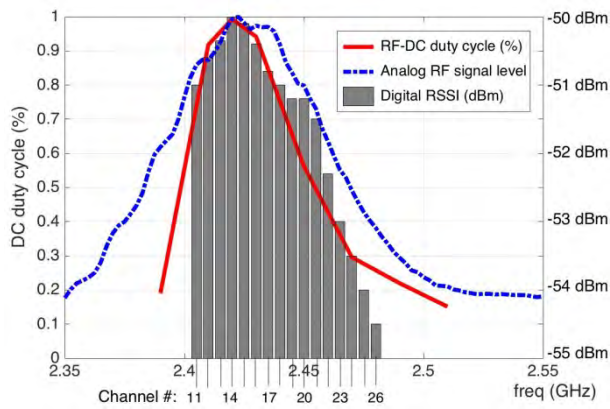
FIGURE 14. Received RSSI for different frequency channels at position D3.

FIGURE 15. Power density at the WSN scenario area for different number of channels used in the WPT system.

the other is attached to the energy harvester. Thus, during the first phase (synchronization), the coordinator sequentially transmits through the LWA data frames with a header indicating which port of the antenna is being used, while performing frequency hopping among the 16 available channels in the 2.405-2.480 GHz band (with 5 MHz step). We assume this band as it is the most widely employed in 802.15.4-based networks. In order to increase the efficiency of this stage, the time schedule for this operation may be pre-defined or negotiated by the motes and the coordinator during the joining process of the formers to the network. With this strategy, the motes are able to wake up and connect to the correct channels at the exact time in which the probe frames are sent by the coordinator, i.e., a synchronization between coordinator and end-nodes is achieved. Thereafter, the motes receive these data frames by their data antennas and measure the RSSI for each transmitting channel and port and stores this information until the end of this synchronization phase. In this way, each node is eventually able to decide the optimum port and frequency channel that provides the highest signal level (RSSI), and to transmit this information back to the network coordinator using the data link. From this moment, once the coordinator has been informed about the most beneficial configuration (port + frequency channel) for each end-node, the energy transfer for each individual mote will be performed following this correspondence. It must be noticed that during the wireless powering phase, the motes receive and store the received energy by using their antennas connected to the harvester. Observe that this two-stage process can be iteratively repeated in order to make the system adaptable to any change in the position of the nodes or perturbations in the radio channel. However, it is expected that in static networks, the synchronization phase needs to be executed only once.

To illustrate this concept, Fig. 14 shows the RSSI measured by a mote located at position D3 as a function of the transmitting channel (#11-#26), together with the RF-to-DC duty cycle obtained from the power harvester for the same position D3. Besides, the analog RF signal level was measured with a microwave network analyzer in a wider frequency span. It can be observed that, as expected, the frequency that
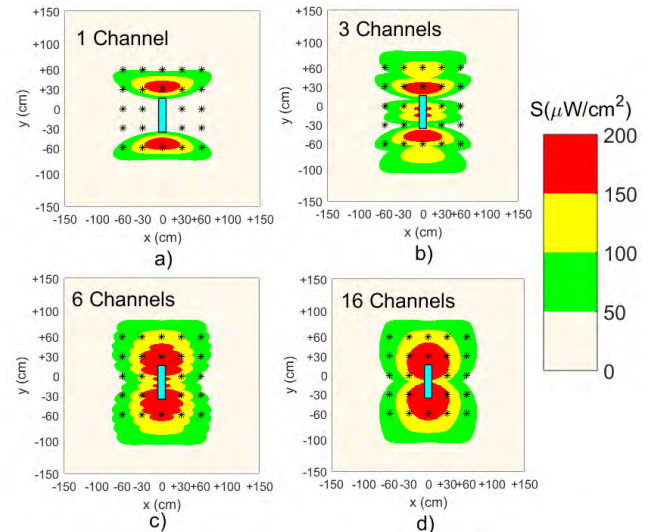
optimizes the DC power transfer in the harvester (2.42 GHz) is the same frequency with maximum analog RF signal, and also it coincides with the frequency channel that provides maximum digital RSSI (channel 14). Thus, Fig. 14 demonstrates the validity of the developed strategy by which a node is capable of estimating the optimum WPT channel for analog RF wireless power transfer using the measured digital RSSI.

Regarding the consumption of energy taken by the channel synchronization stage, note that it can be severely reduced once the aforementioned channel association between the coordinator (energy transmitter) and the end-nodes is achieved. As explained, this process can be pre-configured beforehand or negotiated by both parts during the joining process. Observe that each end-node just needs to be awake and sniffing the corresponding channels during the short and scheduled periods of probe transmissions. It may be also considered the possible repetition of this process more than once, in order to avoid punctual fluctuation of the measured RSSI. This process also enables the use of the proposed system in dynamical WSN, in which the end-nodes may present certain grade of mobility or the propagation conditions might change over the time, as well. These aspects should be individually studied depending on the environmental and system circumstances. After sniffing the channel, the motes only have to send one frame to the coordinator including its preferred configuration. Therefore, it can be seen that this process does not imply a large waste of energy by the end-nodes.

Moreover, in order to reduce the power consumption by the motes when measuring the RSSI and to make the system more efficient, it is important to analyze the minimum number of frequency channels needed to efficiently cover a given WSN area. The fewer number of channels, the lower the time and energy requested to perform the channel sounding. However, a reduced amount of channels could impact the spatial coverage of the RWPT system. This is shown in Fig. 15, which shows the covered power distribution for different
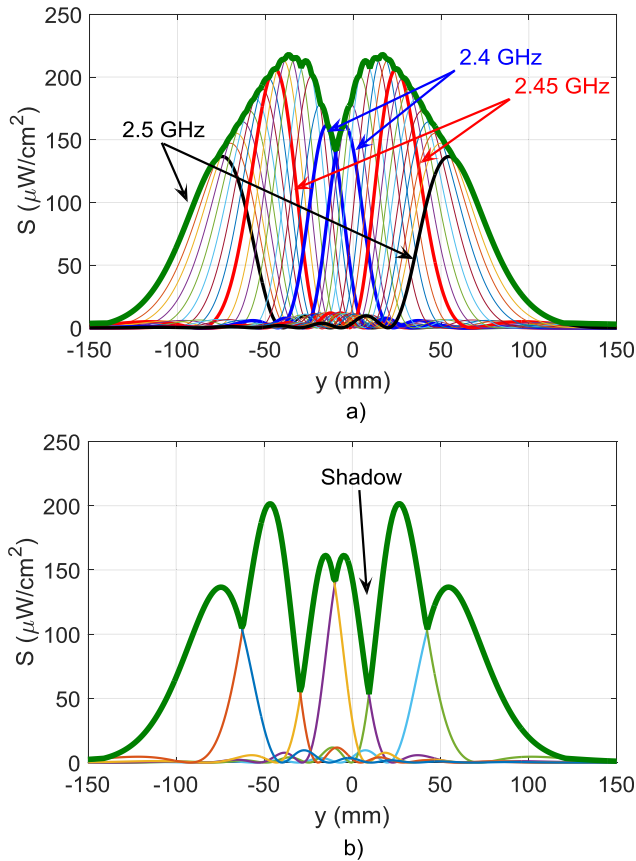
FIGURE 16. Y-direction cut of the coverage for a) 16 channels and b) 3 channels.
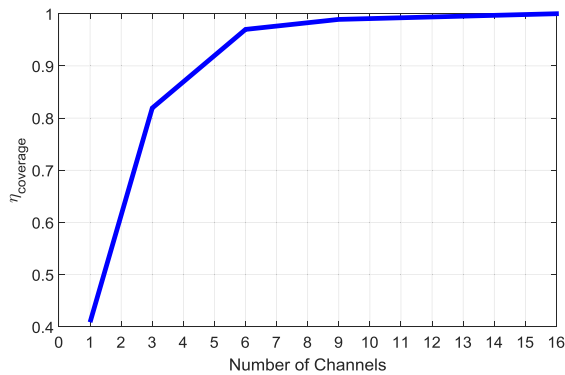

FIGURE 17. Coverage efficiency as a function of the number of channels used in the WPT system.

number of scanning channels. In the first scenario, a single frequency channel is used, so that only two tilted fan regions are illuminated, leaving much of the WSN area without power coverage. As we increase the number of channels, the shadowed zones without power are reduced. In the studied case, 6 channels are needed to cover most of the WSN area. If we increase this amount of scanning channels, the overall WSN power coverage does not significantly improve, as shown in Fig. 15 for 16 channels. Fig. 16 illustrates this shadow effect

showing the coverage cut along the y-direction for 16 and 3 channels. On the other hand, an increased number of requested channels leads to higher time and energy needed to perform the synchronization phase. To better understand this, Fig. 17 shows the coverage efficiency, defined as the ratio between the total coverage using all the 16 channels and the coverage using a given number of channels. In this case the total coverage is calculated as the integral of the power density along the whole area of 1.2×1.2 meters:

$$Coverage_{(Nchannels)} = \int_{-60cm}^{60cm} \int_{-60cm}^{60cm} S_{(Nchannels)}(x, y)dxdy$$

$$(6)$$

As demonstrated in Fig. 17, with just 6 channels, we can achieve an outstanding coverage efficiency $\eta_{COV} > 95\%$, where the coverage efficiency is defined as:

$$\eta_{COV} = \frac{Coverage_{(Nchannels)}}{Coverage_{(N=16)}} \quad (7)$$

This way, the time and power needed in the synchronization phase is reduced with respect to the case of using all 16 available frequency channels. As it was shown in Fig. 15, all the motes can be efficiently illuminated over the threshold of $50\mu W/cm^2$ using only 6 channels of the 16 available channels. Obviously, these channels have been properly selected, using a uniform distribution through the available spectrum, so that the associated spatial distribution is optimum with respect to the total WSN area to be efficiently illuminated and powered.

VIII. CONCLUSION

It has been demonstrated that a fan-beam frequency-scanning antenna together with a channel-hopping technique, can be used as a simple mechanism for adaptive radiative wireless power transfer in a WSN. The beaming efficiency can be dynamically optimized for each node position, using a simple protocol in which the WSN coordinator sweeps frequency of a monitoring signal, and the nodes select the channel with maximum RSSI level. As a proof of concept, this paper has illustrated the capacity to power an IEEE 802.15.4-based WSN with 25 nodes spread in a 1.2 m × 1.2 m area, using its 16 channels in the 2.4 GHz band. This solution is much simpler than other WPT dynamic beaming techniques based on phased-arrays and 2D beaming, and thus can lead to cost-effective solutions to remotely power commercial WSN grids.

REFERENCES

[1] Z. Popović, E. A. Falkenstein, D. Costinett, and R. Zane, "Low-power far-field wireless powering for wireless sensors," *Proc. IEEE*, vol. 101, no. 6, pp. 1397–1409, Jun. 2013.

[2] K. Huang and V. K. N. Lau, "Enabling wireless power transfer in cellular networks: Architecture, modeling and deployment," *IEEE Trans. Wireless Commun.*, vol. 13, no. 2, pp. 902–912, Feb. 2014.

[3] K. Huang and X. Zhou, "Cutting the last wires for mobile communications by microwave power transfer," *IEEE Commun. Mag.*, vol. 53, no. 6, pp. 86–93, Jun. 2015.

[4] L. Xie, Y. Shi, Y. T. Hou, and A. Lou, "Wireless power transfer and applications to sensor networks," *IEEE Wireless Commun.*, vol. 20, no. 4, pp. 140–145, Aug. 2013.

[5] A. Massa, G. Oliveri, F. Viani, and P. Rocca, "Array designs for long-distance wireless power transmission: State-of-the-art and innovative solutions," *Proc. IEEE*, vol. 101, no. 6, pp. 1464–1481, Jun. 2013.

[6] T. D. P. Perera, D. N. K. Jayakody, S. K. Sharma, S. Chatzinotas, and J. Li, "Simultaneous wireless information and power transfer (SWIPT): Recent advances and future challenges," *IEEE Commun. Surveys Tuts.*, vol. 20, no. 1, pp. 264–302, 1st Quart., 2017.

[7] Z. Ding *et al.*, "Application of smart antenna technologies in simultaneous wireless information and power transfer," *IEEE Commun. Mag.*, vol. 53, no. 4, pp. 86–93, Apr. 2015.

[8] M. R. A. Khandaker and K.-K. Wong, "SWIPT in MISO multicasting systems," *IEEE Wireless Commun. Lett.*, vol. 3, no. 3, pp. 277–280, Jun. 2014.

[9] Q. Shi, L. Liu, W. Xu, and R. Zhang, "Joint transmit beamforming and receive power splitting for MISO SWIPT systems," *IEEE Trans. Wireless Commun.*, vol. 13, no. 6, pp. 3269–3280, Jun. 2014.

[10] X. Wang, S. Sha, J. He, L. Guo, and M. Lu, "Wireless power delivery to low-power mobile devices based on retro-reflective beamforming," *IEEE Antennas Wireless Propag. Lett.*, vol. 13, pp. 919–922, 2014.

[11] M. Sheng, L. Wang, X. Wang, Y. Zhang, C. Xu, and J. Li, "Energy efficient beamforming in MISO heterogeneous cellular networks with wireless information and power transfer," *IEEE J. Sel. Areas Commun.*, vol. 34, no. 4, pp. 954–968, Apr. 2016.

[12] Q. Shi, W. Xu, T. H. Chang, Y. Wang, and E. Song, "Joint beamforming and power splitting for MISO interference channel with SWIPT: An SOCP relaxation and decentralized algorithm," *IEEE Trans. Signal Process.*, vol. 62, no. 23, pp. 6194–6208, Dec. 2014.

[13] J. Xu, L. Liu, and R. Zhang, "Multiuser MISO beamforming for simultaneous wireless information and power transfer," *IEEE Trans. Signal Process.*, vol. 62, no. 18, pp. 4798–4810, Sep. 2014.

[14] B. K. Chalise, H. A. Suraweera, G. Zheng, and G. K. Karagiannidis, "Beamforming optimization for full-duplex wireless-powered MIMO systems," *IEEE Trans. Commun.*, vol. 65, no. 9, pp. 3750–3764, Sep. 2017.

[15] Q. Shi, C. Peng, W. Xu, M. Hong, and Y. Cai, "Energy efficiency optimization for MISO SWIPT systems with zero-forcing beamforming," *IEEE Trans. Signal Process.*, vol. 64, no. 4, pp. 842–854, Feb. 2016.

[16] Z. Deng, Y. Gao, W. Li, and C. Cai, "Robust secure beamforming for SWIPT systems with full-duplex receivers and energy-harvesting eavesdroppers," in *Proc. IEEE Int. Conf. Consum. Electron. (ICCE-TW)*, Jun. 2017, pp. 217–218.

[17] D. Schemmel and P. Nayeri, "A smart wireless energy harvesting system with adaptive beamforming and power management," in *Proc. IEEE Int. Symp. Antennas Propag. USNC/URSI Nat. Radio Sci. Meeting*, Jul. 2017, pp. 1085–1086.

[18] M. Ali, G. Yang, and R. Dougal, "A new circularly polarized rectenna for wireless power transmission and data communication," *IEEE Antennas Wireless Propag. Lett.*, vol. 4, pp. 205–208, 2005.

[19] F. Viani, G. Oliveri, and A. Massa, "Compressive sensing pattern matching techniques for synthesizing planar sparse arrays," *IEEE Trans. Antennas Propag.*, vol. 61, no. 9, pp. 4577–4587, Sep. 2013.

[20] L. Poli, T. Moriyama, and P. Rocca, "Pulse splitting for harmonic beamforming in time-modulated linear arrays," *Int. J. Antennas Propag.*, vol. 2014, Jun. 2014, Art. no. 797590.

[21] D. Masotti, A. Costanzo, M. Del Prete, and V. Rizzoli, "Time-modulation of linear arrays for real-time reconfigurable wireless power transmission," *IEEE Trans. Microw. Theory Techn.*, vol. 64, no. 2, pp. 331–342, Jan. 2016.

[22] M. Ettore, W. A. Alomar, and A. Grbic, "2-D Van Atta array of wide-band, wideangle slots for radiative wireless power transfer systems," *IEEE Trans. Antennas Propag.*, vol. 66, no. 9, pp. 4577–4585, Sep. 2018.

[23] Y. Li and V. Jandhyala, "Design of retrodirective antenna arrays for short-range wireless power transmission," *IEEE Trans. Antennas Propag.*, vol. 60, no. 1, pp. 206–211, Jan. 2012.

[24] Y.-J. Ren and K. Chang, "New 5.8-GHz circularly polarized retrodirective rectenna arrays for wireless power transmission," *IEEE Trans. Microw. Theory Techn.*, vol. 54, no. 7, pp. 2970–2976, Jul. 2006.

[25] S. Trinh-Van, J. M. Lee, Y. Yang, K.-Y. Lee, and K. C. Hwang, "Improvement of RF wireless power transmission using a circularly polarized retrodirective antenna array with EBG structures," *Appl. Sci.*, vol. 8, no. 3, p. 324, 2018.

[26] K. W. Choi, P. A. Rosyady, L. Ginting, A. A. Aziz, D. Setiawan, and D. I. Kim, "Theory and experiment for wireless-powered sensor networks: How to keep sensors alive," *IEEE Trans. Wireless Commun.*, vol. 17, no. 1, pp. 430–444, Jan. 2018.

[27] N. B. Carvalho *et al.*, "Europe and the future for WPT COST action IC1301 team," *IEEE Microw. Mag.*, vol. 18, no. 4, pp. 56–87, May 2017.

[28] M. Donelli, P. Rocca, and F. Viani, "Design of a WPT system for the powering of wireless sensor nodes: Theoretical guidelines and experimental validation," *Wireless Power Transf.*, vol. 3, no. 1, pp. 15–23, 2016.

[29] A. A. Oliner and D. R. Jackson, "Leaky-wave antennas," in *Antenna Engineering Handbook*, 4th ed., J. L. Volakis, Ed. New York, NY, USA: Mc-Grow-Hill, 2007.

[30] C. A. Balanis, *Antenna Theory: Analysis and Design*, 3rd ed. Hoboken, NJ, USA: Wiley, 2005.

[31] *Interline Panel Antenna*. Accessed: Oct. 31, 2018. [Online]. Available: https://interline.pl/antennas/PANEL-14-2.4GHz

[32] R. C. Hansen, "Array pattern control and synthesis," *Proc. IEEE*, vol. 80, no. 1, pp. 141–151, Jan. 1992.

[33] R. S. Elliott, "On discretizing continuous aperture distributions," *IEEE Trans. Antennas Propag.*, vol. 25, no. 5, pp. 617–621, Sep. 1977.

[34] R. E. Hodges and Y. Rahmat-Samii, "On sampling continuous aperture distributions for discrete planar arrays," *IEEE Trans. Antennas Propag.*, vol. 44, no. 11, pp. 1499–1508, Nov. 1996.

[35] M. Poveda-García, J. L. Gómez-Tornero, and D. Cañete-Rebenaque, "Study of the efficiency of half-width substrate integrated waveguide leaky-wave antennas in FR4," in *Proc. 2nd URSI AT-RASC*, May 2018, pp. 1–4.

[36] *Powercast's P21XX Powerharvester Evaluation Kit*. Accessed: Oct. 31, 2018. [Online]. Available: http://www.powercastco.com/products/development-kits/

[37] *Atmel AVR2162: REB233SMAD—Hardware User Manual*. Accessed: Oct. 31, 2018. [Online]. Available: http://ww1.microchip.com/downloads/en/AppNotes/doc42006.pdf

[38] *Promax FA-363C DC Source*. Accessed: Oct. 31, 2018. [Online]. Available: http://www.promaxelectronics.com/ing/products/power-supplies/FA-363C/30V-5A-multi-output-power-supply-plus-fixed-outputs-5V-15V.

[39] *RFPA5201E Power Amplifier*. Accessed: Oct. 31, 2018. [Online]. Available: https://www.qorvo.com/products/p/RFPA5201E

[40] *Sky13586-678LF*. Accessed: Oct. 31, 2018. [Online]. Available: http://www.skyworksinc.com/Product/3296/SKY13586-678LF?source=npa

[41] P. S. Hall and S. J. Vetterlein, "Review of radio frequency beamforming techniques for scanned and multiple beam antennas," *IEE Proc. H-Microw., Antennas Propag.*, vol. 137, pp. 293–303, Oct. 1990.

[42] A. Boaventura, A. Collado, N. B. Carvalho, and A. Georgiadis, "Optimum behavior: Wireless power transmission system design through behavioral models and efficient synthesis techniques," *IEEE Microw. Mag.*, vol. 14, no. 2, pp. 26–35, Mar. 2013.

[43] A. Boaventura and N. B. Carvalho, "Maximizing DC power in energy harvesting circuits using multisine excitation," in *IEEE MTT-S Int. Microw. Symp. Dig.*, Jun. 2011, pp. 1–4.

[44] A. J. S. Boaventura, A. Collado, A. Georgiadis, and N. B. Carvalho, "Spatial power combining of multi-sine signals for wireless power transmission applications," *IEEE Trans. Microw. Theory Techn.*, vol. 62, no. 4, pp. 1022–1030, Apr. 2014.

[45] D. Mishra *et al.*, "Smart RF energy harvesting communications: Challenges and opportunities," *IEEE Commun. Mag.*, vol. 53, no. 4, pp. 70–78, Apr. 2015.

MIGUEL POVEDA-GARCÍA was born in Pozohondo, Spain, in 1992. He received the telecommunications engineering degree and the master's degree in telecommunications engineering from the Technical University of Cartagena, Cartagena, Spain, in 2014 and 2016, respectively, where he is currently pursuing the Ph.D. degree. His Ph.D. study is focused on the analysis of the dispersion of planar leaky-wave antennas in substrate integrated waveguide technology and their design for different applications. His research interests include leaky-wave antennas and their application in telecommunication systems, the Internet of Things, and energy harvesting.

JORGE OLIVA-SÁNCHEZ was born in Murcia, Spain, in 1982. He received the telecommunications engineering degree from the Technical University of Cartagena, Spain, in 2006. He is currently pursuing the Ph.D. degree with the Technical University of Cartagena. He received a Leonardo Da Vinci grant from Whitfield Solar Ltd., U.K., for research in new solar photovoltaic concentrators, in 2006. In 2008, he joined the National Technical Aerospace Institute as a Technical Engineer for national and international projects in the aerospace sector, working in airborne and satellite electrical devices and European navigation programs.

His work in the European Galileo program resulted in a seconded national expert position with the European GNSS Agency, from 2013 to 2015. His main research interests include analysis of wireless power transfer for sensor networks and SWIPT systems.
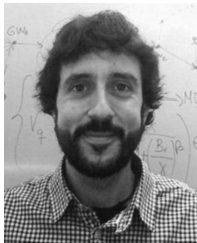
RAMON SANCHEZ-IBORRA is currently an Assistant Professor and a Researcher with the Information and Communications Engineering Department, University of Murcia, Spain. received the B.Sc. degree in telecommunication engineering and the M.Sc. and Ph.D. degrees in information and communication technologies from the Technical University of Cartagena, Spain, in 2007, 2013, and 2016, respectively. He has also been a Visiting Pre-Doctoral Researcher with the NetGNA Research Group, University of Beira Interior, Portugal, in 2014, and with the Quality and Usability Laboratory, Technical University of Berlin/Telekom Innovation Laboratories, Germany, in 2015. He has been an Invited Professor with the Engineering Faculty of the University of Quindío, Colombia, since 2017, and a Post-Doctoral Visiting Researcher with the ARTS Research Group, Mediterranean University, Reggio Calabria, Italy. His main research interests are evaluation of QoE in multimedia services, management of wireless mobile networks, green networking techniques, and IoT/M2M architectures. He has published several papers in national and international conferences and journals. He is a member of many IEEE technical committees. He has collaborated as a TPC member and reviewer for international journals and conferences, such as the IEEE ICC, EAI ADHOCNETS, and the *IEEE Communications Magazine*.

DAVID CAÑETE-REBENAQUE was born in Valencia, Spain, in 1976. He received the telecommunications engineering degree from the Technical University of Valencia, Valencia, in 2000, and the Ph.D. degree from the Technical University of Cartagena, Cartagena, Spain, in 2009. In 2001, he joined as an RF Engineer with Mobile Communication Company. In 2002, he joined the Communications and Information Technologies Department, Technical University of Cartagena, where he currently is involved in research and teaching activities. His current research interests include the analysis and design of microwave circuits and antennas.

JOSÉ LUIS GÓMEZ-TORNERO (SM'01–M'06–SM'14) was born in Murcia, Spain, in 1977. He received the telecommunications engineering degree from the Technical University of Valencia, Valencia, Spain, in 2001, and the Ph.D. degree from the Technical University of Cartagena (UPCT), Cartagena, Spain, in 2005. In 2000, he joined the Radio Frequency Division, Industry Alcatel Espacio, Madrid, Spain. In 2001, he joined UPCT, where he has been an Associate Professor, since 2008. He was the Vice Dean for Students and Lectures affairs as a member of the Telecommunication Engineering Faculty. He has been a Visiting Researcher/Professor with the University of Loughborough, Loughborough, U.K., Heriot-Watt University, Edinburgh, U.K., Queen's University Belfast, Belfast, U.K., and the CSIRO-ICT Centre, Sydney, NSW, Australia. In 2010, he was appointed as CSIRO Distinguished Visiting Scientist by the CSIRO ICT Centre.

He has co-authored more than 50 peer-reviewed journal papers, and more than 100 conference papers. His current research interests include the analysis and design of leaky-wave devices and their applications, and the innovation in the area of higher education.

His research work has received various awards, including the EPSON-Ibérica Foundation Award and the Vodafone Foundation Award for the Best Ph.D. Thesis in the area of advanced mobile communications technologies, in 2004 and 2005, respectively, and the Hispasat Proze and Hisdesat Prize for the Best Ph.D. Thesis in Satellite Communication Technologies, in 2014 and 2015, respectively. He was also a co-recipient of the 2010 IEEE Engineering Education Conference Award, the 2011 EuCAP Best Student Paper Prize, the 2012 EuCAP Best Antenna Theory Paper Prize, the 2012 and 2013 Spanish URSI Prize for the Best Student Paper, the 2013 APS Best Student Paper Finalist, and the 2018 iWAT Best Poster Award.

• • •